

# Sharp transitions in rotating turbulent convection: Lagrangian acceleration statistics reveal a second critical Rossby number

Kim M. J. Alards,<sup>1</sup> Rudie P. J. Kunnen,<sup>1</sup> Richard J. A. M. Stevens,<sup>2</sup>  
Detlef Lohse,<sup>2,3</sup> Federico Toschi,<sup>1,4,5</sup> and Herman J. H. Clercx<sup>1,\*</sup>

<sup>1</sup>*Fluid Dynamics Laboratory and J.M. Burgers Center for Fluid Dynamics,  
Department of Applied Physics, Eindhoven University of Technology,  
P.O. Box 513, 5600 MB Eindhoven, The Netherlands*

<sup>2</sup>*Physics of Fluids Group, Max Planck Center for Complex Fluid Dynamics,  
J.M. Burgers Center for Fluid Dynamics and MESA+ Research Institute,  
Department of Science and Technology, University of Twente,  
P.O. Box 217, 7500 AE Enschede, The Netherlands*

<sup>3</sup>*Max Planck Institute for Dynamics and Self-Organization, Am Fassberg 17, 37077 Göttingen, Germany*

<sup>4</sup>*Centre of Analysis, Scientific Computing, and Applications W&I,  
Department of Mathematics and Computer Science, Eindhoven University of Technology,  
P.O. Box 513, 5600 MB Eindhoven, The Netherlands*

<sup>5</sup>*Istituto per le Applicazioni del Calcolo, Consiglio Nazionale delle Ricerche, Via dei Taurini 19, 00185 Rome, Italy*

In Rayleigh–Bénard convection (RBC) for fluids with Prandtl number  $Pr \gtrsim 1$ , rotation beyond a critical (small) rotation rate is known to cause a sudden enhancement of heat transfer which can be explained by a change in the character of the boundary layer (BL) dynamics near the top and bottom plates of the convection cell. Namely, with increasing rotation rate, the BL signature suddenly changes from Prandtl–Blasius type to Ekman type. The transition from a constant heat transfer to an almost linearly increasing heat transfer with increasing rotation rate is known to be sharp and the critical Rossby number  $Ro_c$  occurs typically in the range  $2.3 \lesssim Ro_c \lesssim 2.9$  (for Rayleigh number  $Ra = 1.3 \times 10^9$ ,  $Pr = 6.7$ , and a convection cell with aspect ratio  $\Gamma = \frac{D}{H} = 1$ , with  $D$  the diameter and  $H$  the height of the cell). The explanation of the sharp transition in the heat transfer points to the change in the dominant flow structure. At  $1/Ro \lesssim 1/Ro_c$  (slow rotation), the well-known large-scale circulation (LSC) is found: a single domain-filling convection roll made up of many individual thermal plumes. At  $1/Ro \gtrsim 1/Ro_c$  (rapid rotation), the LSC vanishes and is replaced with a collection of swirling plumes that align with the rotation axis. In this paper, by numerically studying Lagrangian acceleration statistics, related to the small-scale properties of the flow structures, we reveal that this transition between these different dominant flow structures happens at a second critical Rossby number,  $Ro_{c2} \approx 2.25$  (different from  $Ro_{c1} \approx 2.7$  for the sharp transition in the Nusselt number  $Nu$ ; both values for the parameter settings of our present numerical study). When statistical data of Lagrangian tracers near the top plate are collected, it is found that the root-mean-square (rms) values and the kurtosis of the horizontal acceleration of these tracers show a sudden increase at  $Ro_{c2}$ . To better understand the nature of this transition we compute joint statistics of the Lagrangian velocity and acceleration of fluid particles and vertical vorticity near the top plate. It is found that for  $Ro \gtrsim 2.25$  there is hardly any correlation between the vertical vorticity and extreme acceleration events of fluid particles. For  $Ro \lesssim 2.25$ , on the other hand, vortical regions are much more prominent and extreme horizontal acceleration events are now correlated to large values of positive (cyclonic) vorticity. This suggests that the observed sudden transition in the acceleration statistics is related to thermal plumes with cyclonic vorticity developing in the Ekman BL and subsequently becoming mature and entering the bulk of the flow for  $Ro \lesssim 2.25$ .

## I. INTRODUCTION

Turbulent flows in nature are often driven by temperature gradients, for example, oceanic currents [1, 2] or large-scale flows in the atmosphere [3, 4]. A well known set-up for studying thermally driven turbulence is Rayleigh–Bénard convection (RBC) [5–7], where a confined fluid layer is heated from below and cooled from above. In general, turbulent flows are characterized by random fluctuations, intermittency and a loss of temporal and spatial coherence [8]. Sudden transitions between turbulent states are therefore unexpected in strongly turbulent flows. In RBC, however, sudden transitions between different turbulent states do occur when the set-up is rotated about its vertical axis (see, e.g., [9–19]). These turbulent states are typically characterized by different large-scale coherent flow structures and different

---

\* h.j.h.clercx@tue.nl

Table I: Several values for the critical Rossby number  $Ro_c$  as found in numerical simulations [10, 11, 16] and experiments [11, 12, 14–17]. Note that the estimated value for  $Ro_c$  reported by Wei *et al.* [17] is based on the same dataset as the one reported by Zhong and Ahlers for the case with  $Pr = 4.38$  [12, 15]. For all these cases convection cells with  $\Gamma = 1$  are considered. The critical Rossby number is an estimate obtained from each of these studies and these data indicate that  $2.3 \lesssim Ro_c \lesssim 2.9$  (for the range of Rayleigh and Prandtl numbers considered in these studies).

Reference	$Ra$	$Pr$	$Ro_c$
Kunnen <i>et al.</i> [10]	$1.0 \times 10^9$	6.4	2.5
Stevens <i>et al.</i> [11]	$2.73 \times 10^8$	6.26	2.6
Zhong <i>et al.</i> [15]	$2.19 \times 10^9$	6.26	2.9
Weiss <i>et al.</i> [14]	$2.25 \times 10^9$	4.38	2.4
Stevens <i>et al.</i> [16]	$2.91 \times 10^8$	4.38	2.5
Zhong <i>et al.</i> [12, 15]	$2.25 \times 10^9$	4.38	2.4
Wei <i>et al.</i> [17]	$2.3 \times 10^9$	4.38	2.3
Present work	$1.30 \times 10^9$	6.70	2.7

heat transfer properties. Not only in rotating RBC, but also in Taylor–Couette and Von Kármán flows transitions between different turbulent states are observed [20–23]. In a Taylor–Couette flow, i.e. the flow between two concentric co- or counter-rotating cylinders, a transition to a different scaling regime sets in when the boundary layers (BLs) become turbulent. This is known as the ultimate regime [21]. It was recently shown that even beyond this transition at high Reynolds numbers multiple states of turbulence are possible [21, 24]. In a Von Kármán flow generated between two counter-rotating disks, bifurcations between turbulent states occur, which are characterized by different coherent flow structures [22, 23]. Like in the Taylor–Couette flow, these states can coexist at high Reynolds numbers [22].

Here, we focus on the transition in rotating RBC (in convection cells with aspect ratio  $\Gamma = \frac{D}{H} = 1$ , with  $D$  the diameter and  $H$  the height of the cell) from a rotation-unaaffected regime, where the heat transfer is constant, to a rotation-affected regime where the heat transfer is enhanced [9–12, 25–28]. At this transition, the boundary layers change from the passive Prandtl–Blasius type to the active Ekman type [18, 29, 30]. The flow structures change drastically, from the domain-filling large scale circulation (LSC) in absence of rotation (or very mild rotation rates) to the emergence of a collection of vertically-aligned vortical plumes [10, 31, 32] at higher rotation rates. Exactly this transition in the BL dynamics is expected to be responsible for the increase in the heat transfer efficiency: in rotating flows strong vortical plumes emerge from the Ekman BL, transporting warm (cold) fluid from the BL at the bottom (top) plate into the bulk flow and enhancing the heat transfer [11, 25, 26, 33, 34]. This mechanism is referred to as Ekman pumping. The traditional view [35] is that the dominant transition in the flow structure (from LSC to vertically-aligned vortices) happens at  $Ro_c$ . Here we show that this transition takes place at a different Rossby number, here denoted by  $Ro_{c2}$ .

It is thus expected that the dynamics of thermal plumes emerging from the BLs majorly determines the heat transfer efficiency. In the Prandtl–Blasius type BL, sheet-like plumes develop, while in the Ekman type BL vortical plumes emerge, characterized by spiraling fluid motion inside the vortex tubes. The plume dynamics in both the rotation-unaaffected and the rotation-affected regime has been investigated before. Few of these studies focused on the vorticity signature of these plumes, and in particular the presence of vertical vorticity. For example, in [36] geometrical characteristics of the sheet-like plumes emerging from the Prandtl–Blasius BL are studied and it is shown that these plumes are typically characterized by large positive and large negative values of the vertical vorticity. In the rotation-affected regime, on the contrary, vortical plumes are characterized by cyclonic (i.e., positive) vorticity only and spiraling fluid motions near the horizontal plates [25, 28, 31]. Vertical vorticity might thus be used to distinguish the plume character outside the BL for the two regimes.

For completeness it is worthwhile to mention that another transition exists in rapidly-rotating RBC, which should not be confused with the transition being considered in this investigation: the transition from the rotation-affected to the rotation-dominated (or geostrophic) regime [37–41]. Knowledge about this regime is still limited. Three main mechanisms have been proposed to explain this transition. King *et al.* [37] hypothesized that the transition from the rotation-affected to the geostrophic regime depends on the relative thickness of the viscous and thermal boundary layers,  $\delta_\nu$  and  $\delta_T$ , respectively. With water as working fluid (with  $Pr > 1$ ) they showed that  $\delta_\nu \gtrsim \delta_T$  for the rotation-affected regime, and  $\delta_\nu \lesssim \delta_T$  for the geostrophic regime. The transition between both regimes then occurs when  $\delta_\nu \approx \delta_T$ . Julien *et al.* [38] suggested that the transition occurs when the vortical plumes span throughout the entire domain (with the bulk becoming fully rotation-dominated) resulting in suppression of vertical motion and thus reduction of heat transfer. Recently, Rajaei and coworkers [41] provided evidence that the transition from rotation-affected to the geostrophic regime occurs when fluid motion in the vertically-aligned vortices becomes decorrelated from the bulk fluid motion between these vortical plumes.

The transition in heat transfer efficiency when passing from the rotation-unaaffected to the rotation-affected regime has been explored in great detail in recent years with laboratory experiments and numerical simulations. A summary of the main results with respect to the critical Rossby number (the ratio of the inertial force to the Coriolis force) for the transition is provided in Table I. It can be concluded that  $2.3 \lesssim Ro_c \lesssim 2.9$  for the range of Rayleigh numbers  $Ra$ , which is a measure for the ratio of buoyancy to viscous forces, and the Prandtl numbers  $Pr$ , the ratio of kinematic viscosity to the thermal diffusion coefficient, typical for laboratory experiments on turbulent convection with water as working fluid. Although the value of  $Ro_c$  varies a bit from one experiment to another and also differs somewhat when compared to simulations (the precise values are also affected by the particular method to determine this critical Rossby value, which are relatively rough estimates in many cases), one of the most remarkable observations is the sharpness of this transition, see in particular Refs. [14, 17] and the other cited works in Table I. Although the transition in the heat transfer due to Ekman pumping is accepted to be sharp, it is not yet clear whether and how this transition is reflected in the modified flow structures (from LSC to vertically-aligned vortices) in general, the plume dynamics in particular, and the emergence and penetration of these structures in the bulk just outside the BLs. Moreover, there is no a priori reason to expect a change in the dominant flow structures at exactly the same rotation rate where the change in heat transfer efficiency is observed. The heat transfer is, moreover, an integral quantity, while flow structures are characterized and quantified by local flow properties, for example, fluid particle velocity and acceleration (and its higher order statistics), geometrical properties of tracer trajectories, (vertical) vorticity, etc. However, since the heat transfer is expected to be related to the typical flow structures and plume dynamics, one might expect that also these local flow quantities are affected by the transition. The question is whether this transition in the behavior of local flow quantities occurs at the same critical Rossby number  $Ro_c$ , or does it require a somewhat different rotation rate to suddenly change the behavior of such local flow quantities? Alternatively, one could imagine that the transition proceeds more gradually outside the BLs as the vortical plumes can gradually penetrate further into the bulk with increasing rotation.

To study coherent structures in turbulent flows, a Lagrangian approach has shown to be particularly useful [42, 43]. An interesting quantity is the acceleration of passive tracers, providing information on the small-scale flow structures and the temporal fluctuations in these flow structures. High acceleration events typically occur in intense vortex filaments [44–46] and are correlated to small-scale intermittency [43, 47]. Rotation is changing the flow structures in turbulent flows both at large and small scales [32] and is therefore expected to modify the acceleration statistics. The effect of rotation on the (small-scale) flow structures in rotation-affected RBC is most prominent near the plates [32]. In this region of the flow thermal plumes develop from the BLs, resulting in highly accelerating fluid parcels. The nature of the thermal plumes changes with the BL transition under rotation [33], from sheet-like in the weakly rotating regime to vertically-aligned vortical plumes in the rotation-affected regime, and a signature of this transition is certainly expected to be visible in the Lagrangian acceleration statistics in rotating RBC.

Acceleration statistics of passive tracers in rotating turbulence have recently been studied experimentally [18, 48]. In [48], rotation was found to widen the tails of the horizontal acceleration PDFs in the bulk of isothermally forced rotating turbulence, while it suppresses the intermittency of the vertical Lagrangian acceleration statistics, i.e. in the direction parallel to the rotational axis. In rotating RBC, acceleration fluctuations in the horizontal direction are found to be enhanced by rotation at the transition from the rotation-unaaffected to the rotation-affected regime, see Ref. [18]. In that paper [18], it was shown that this transition towards a more intermittent acceleration is related to the transition in the BLs from the Prandtl–Blasius type to the Ekman type. In particular, the spiraling motion of plumes developing in the Ekman BL enhances the horizontal component of the acceleration. Within the resolution of the Rossby number used in [18], a gradual transition in the Lagrangian statistics of acceleration was observed. The gradual change of the Lagrangian statistics has not been explored in more detail in that particular study, although it was somewhat unexpected, given that the (related) transition in the heat transfer is known to be sharp.

Here, we will extend the experimental study of Ref. [18] numerically by zooming in on the transition in the Lagrangian acceleration statistics in order to better understand the flow dynamics around this transition and the relation between the Lagrangian velocity and acceleration of fluid particles and the thermal plumes. We collect these Lagrangian velocity and acceleration statistics in rotating RBC using direct numerical simulations (DNS) over a considerable range of rotation rates, between  $Ro = 0.058$  and  $Ro = \infty$  (no rotation). In particular, we enhance the resolution of measurement points (Rossby numbers) around the anticipated transition at  $Ro_c$  observed in the heat transfer, which from now on will be denoted as  $Ro_{c_1}$  as maybe a second critical Rossby number may occur. Different regions of the flow are explored and fluid particle velocity, acceleration and vorticity statistics measured in the center of the convection cell are compared to similar statistical quantities measured near the top plate (including the BL, but with a substantial measurement region outside the BL). The advantage of using DNS is that the flow field (an Eulerian dataset) and the fluid particle trajectories (a Lagrangian dataset) are available simultaneously, so that we can also make a direct connection between the Lagrangian velocity and acceleration statistics and the characteristics of the underlying flow field such as the (vertical) vorticity. In this work, the focus is on finding the critical Rossby number for the transition in the dominant flow structures (which we denote here by  $Ro_{c_2}$  as we cannot assume a

priori that this critical Rossby number is the same as the one mentioned above and denoted by  $Ro_{c_1}$ ) and the possible abruptness of such a transition in terms of the critical Rossby number  $Ro_{c_2}$ , and it is based on *Lagrangian statistics data*, in particular the autocorrelation fluctuations and higher-order statistics. Additionally, we report signatures of the transition in the flow structures close to the plates in rotating RBC.

The paper is organized as follows: In Section II we introduce the numerical method used in this investigation. Results with regard to the transition in the heat transfer and the acceleration statistics, and transitions in the flow structures near the top plate, are presented and discussed in Section III. Section IV contains a summary and the main conclusions.

## II. NUMERICAL METHOD

We have performed DNS of a (rotating) cylindrical Rayleigh–Bénard system. The governing dimensionless equations are the incompressible Navier–Stokes equations with the Coriolis term, and the energy equation, both in the Boussinesq approximation:

$$\nabla \cdot \mathbf{u} = 0, \quad (1)$$

$$\frac{\partial \mathbf{u}}{\partial t} + (\mathbf{u} \cdot \nabla) \mathbf{u} + \frac{1}{Ro} \hat{\mathbf{z}} \times \mathbf{u} = -\nabla p + \sqrt{\frac{Pr}{Ra}} \nabla^2 \mathbf{u} + T \hat{\mathbf{z}}, \quad (2)$$

$$\frac{\partial T}{\partial t} + (\mathbf{u} \cdot \nabla) T = \frac{1}{\sqrt{PrRa}} \nabla^2 T, \quad (3)$$

with  $\mathbf{u}$  the velocity vector,  $t$  time,  $p$  pressure,  $T$  temperature and  $\hat{\mathbf{z}}$  the vertical unit vector. These equations are non-dimensionalized using the cell height  $H$  for length,  $\Delta T$  (the temperature difference between the bottom and top plate) for temperature, and  $t_c = H/U$  for time, based on the free-fall velocity  $U \equiv \sqrt{g\alpha\Delta T H}$ , where  $g$  is the gravitational acceleration and  $\alpha$  is the thermal expansion coefficient of the fluid. The corresponding dimensionless numbers are the Rayleigh number  $Ra = g\alpha\Delta TH^3/(\nu\kappa)$ , the Prandtl number  $Pr = \nu/\kappa$ , and the Rossby number  $Ro = U/(2\Omega H)$ , with  $\nu$  and  $\kappa$  the kinematic viscosity and thermal diffusivity of the fluid, respectively, and  $\Omega$  the rotation rate. We simulate a cylinder with aspect ratio  $\Gamma = D/H = 1$ , with  $D$  the diameter of the cell. We solve the equations in cylindrical coordinates using a second-order finite difference scheme that is described in detail in [49, 50]. For the discretization  $512 \times 384 \times 512$  grid points are used in the azimuthal, radial, and axial direction, respectively. To ensure that there are at least ten grid points within the boundary layer, grid refinement towards the walls is used in both the vertical and radial directions. The boundary conditions (BCs) are no-slip BCs at all walls, a fixed temperature BC at the top/bottom horizontal walls and adiabatic BCs (i.e. absence of heat flux) at the sidewalls. The other control parameters are set as  $Ra = 1.3 \times 10^9$ ,  $Pr = 6.7$  (corresponding to water) and the Rossby number is varied between  $0.058 \leq Ro \leq \infty$ , where  $Ro = \infty$  is the non-rotating case.

Inside the RBC flow passive tracers, following the fluid motion exactly, are tracked. To interpolate the fluid velocity from the surrounding eight grid points around the particle position, we use a tri-linear interpolation scheme and for the time integration a second-order Adams–Bashforth scheme is used. Lagrangian acceleration statistics of  $10^6$  passive tracers are collected in two different measurement volumes; one of size  $0.25H \times 0.25H \times 0.25H$  placed in the center of the cell and one of size  $0.25H \times 0.25H \times 0.05H$  placed under the top plate as sketched in figure 1. This top measurement volume is attached to the top plate such that it spans the range  $0.95H < z < H$  vertically, while it is centered around  $r = 0$  horizontally. In order to obtain error estimates we use the symmetry of the flow problem with respect to the plane  $z = 0.5H$  and compare statistical data obtained for  $z > 0.5H$  with those obtained for  $z < 0.5H$ . For the symmetric domain in the center this can be implemented in a straightforward way. We also analysed Lagrangian acceleration statistics of passive tracers in a similar domain near the bottom plate, spanning the vertical range  $0 < z < 0.05H$ , to complement the data from the volume just below the top plate. We will in addition collect more local statistics in horizontal slabs of thickness  $\Delta z_i = 0.001H$  and different vertical positions  $z_i$ .

## III. RESULTS AND DISCUSSION

### A. Transition in the heat transfer

For the set of parameters studied here, it is known that there is a sharp transition in the heat transfer around a critical Rossby number  $Ro_c$  in the range  $2.3 \lesssim Ro \lesssim 2.9$  [10, 12, 17, 27], see also Table I. The heat transfer is expressed by the Nusselt number  $Nu$ , giving the ratio between the total heat transfer and the convective heat transfer. In (rotating) RBC, the Nusselt number averaged over the full volume can be written as  $Nu = 1 + \sqrt{PrRa}\langle u_z T \rangle$ ,

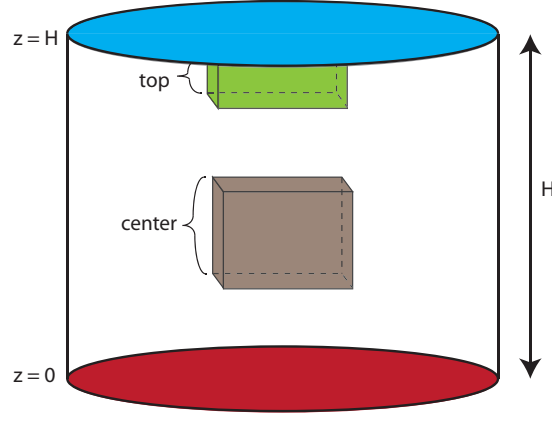


Figure 1: Sketch of the measurement volumes (not to scale). The gray cube in the center represents a measurement volume of size  $0.25H \times 0.25H \times 0.25H$ , in the  $x$ -,  $y$ - and  $z$ -direction, respectively. The green rectangular parallelepiped at the top plate represents a measurement volume of size  $0.25H \times 0.25H \times 0.05H$  that starts right under the top plate (spanning the range  $0.95H < z < H$  vertically).

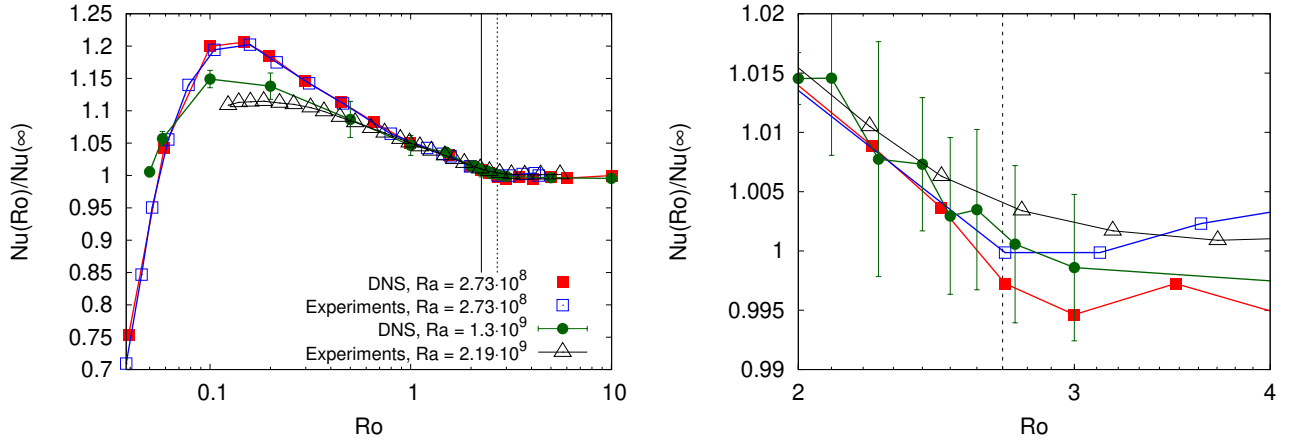


Figure 2: a) The Nusselt number  $Nu$  as function of  $Ro$ , normalized by  $Nu(\infty)$  for the non-rotating case. Squares show data from [11, 12] for  $Ra = 2.73 \times 10^8$  and  $Pr = 6.26$ , circles show data for the current simulations at  $Ra = 1.3 \times 10^9$  and  $Pr = 6.7$ , and triangles show experimental data by [15] (supplementary data) taken at  $Ra = 2.19 \times 10^9$  and  $Pr = 6.26$ . Closed symbols are for DNS while the open symbols are for experiments. b) The same datasets, but now showing a zoom of the data in the range  $2 \leq Ro \leq 4$ . The vertical dotted line in both panels represents  $Ro_{c1} = 2.7$ , and the vertical solid line in the left panel represents  $Ro_{c2} = 2.25$ .

where  $u_z$  is the vertical fluid velocity. In figure 2, we show this Nusselt number as a function of  $Ro$  from the current simulations and from data reported in [11, 12, 15]. We observe a transition from the constant heat transfer regime (where  $Nu(Ro)/Nu(\infty) \approx 1$ ) to an enhanced heat transfer regime at  $Ro_{c1} \approx 2.7$ , presented by the dotted line (here, we introduce the critical Rossby number  $Ro_{c1}$  for the specific case explored in this study). Note that for the current discussion there is no need to pinpoint the exact position of the transition.

## B. Acceleration statistics

As mentioned in the Introduction, we will supplement the work of Rajaei *et al.* [18], where trajectories of neutrally buoyant particles are reconstructed in experiments of rotating RBC with  $Ra = 1.3 \times 10^9$  and  $Pr = 6.7$ , by numerical simulations. In these numerical simulations the resolution in the Rossby number around  $Ro_{c_1}$  is increased compared to the investigation reported in Ref. [18] to have a closer look at the position of the transition in terms of the Lagrangian acceleration statistics (and possibly disclosing its sharpness). Given that the flow structures in and nearby the BLs at the horizontal plates are expected to drive the transition, we will compare Lagrangian statistics collected both in the center of the convection cell and in the top measurement volume as in [18]. To understand how the fluctuations in the vertical and horizontal components of the acceleration change under rotation, we will first focus on the root-mean-square (rms) values of the horizontal and vertical acceleration. Then the kurtosis and skewness measurements are discussed. The kurtosis of the acceleration probability density function (PDF) gives an indication of the presence of extreme acceleration events and with the skewness of the acceleration PDF we can explore whether the Lagrangian acceleration statistics are symmetric or asymmetric.

### 1. Root-mean-square values of acceleration

The rms values of the horizontal and vertical acceleration are computed as  $a_i^{rms} = \sqrt{\langle (a_i - \langle a_i \rangle)^2 \rangle}$ , where  $i = xy$  or  $i = z$  and the average is taken over time and over the top and center measurement volumes, respectively, as sketched in figure 1. For the horizontal component,  $a_{xy}^{rms}$ , the average is taken over a statistical sample that includes the values of both  $a_x$  and  $a_y$  because the statistical properties of the turbulent flow are assumed to be homogeneous and isotropic in the horizontal direction (and cannot depend on the orientation of the horizontal coordinate axes). As already discussed in [18] and shown by previous experiments on rotating turbulence [48], rotation decreases the acceleration intensity along the rotational axis. Indeed,  $a_z^{rms}$  is found to decrease with decreasing  $Ro$  both in the center and near the top plate when  $Ro \lesssim 1.0$ . However, and in contrast to [48], weak maxima in  $a_z^{rms}$  are observed in rotating RBC which are positioned at  $Ro \approx 2$  and  $Ro \approx 1$  for the central and top measurement volumes, respectively. Note that these maxima do not coincide with the critical Rossby number  $Ro_{c_1} \approx 2.7$  at which we observe the transition in heat transfer. With increasing rotation rate (decreasing  $Ro$ ), the rms of the horizontal acceleration component  $a_{xy}^{rms}$  in the center of the convection cell first slightly increases up to  $Ro \approx 1$  and then decreases subsequently. This trend is opposite to what has been reported for rotating turbulence by [48]. Near the top plate  $a_{xy}^{rms}$  increases significantly with increasing rotation rate, due to the formation of vortical plumes with swirling horizontal motion in the Ekman BLs. As observed in the inset of figure 3a, this transition to increasing  $a_{xy}^{rms}$  near the top plate is quite sudden and occurs at  $Ro_{c_2} \approx 2.25$ , where  $Ro_{c_2}$  is represented by the vertical solid line. The fact that this transition is more prominent for the rms values of horizontal accelerations points at an increase of the anisotropy of acceleration with increasing rotation for  $Ro \lesssim 2.25$ . We quantify this in terms of the ratio between the horizontal and vertical acceleration components,  $R_{a^{rms}} = a_{xy}^{rms}/a_z^{rms}$ , shown in figure 3b. As already found in the experiments of Ref. [18], in the center of the convection cell this ratio is almost independent of the rotation rate and shows, near the top plate, a transition from an approximately constant anisotropy ratio  $R_{a^{rms}} = a_{xy}^{rms}/a_z^{rms} \approx 1$  in the weakly rotating cases ( $Ro \gtrsim 2.25$ ) to a trend with significant increase of the anisotropy ratio  $R_{a^{rms}}$  for  $Ro \lesssim 2.25$ . In the inset of figure 3b, we show that also this transition at  $Ro_{c_2}$  is quite abrupt.

### 2. Kurtosis and skewness of acceleration

The probability density functions (PDFs) of acceleration in turbulent flows are characterized by exponential tails [47, 51]. In (rotating) RBC, the coherent flow structures are influencing the tails of the acceleration PDFs [18]. The relative importance of the tails in such a PDF can be quantified by the kurtosis,  $K_i = \langle (a_i - \langle a_i \rangle)^4 \rangle / \langle (a_i - \langle a_i \rangle)^2 \rangle^2$ , where the average is taken over volume and time. Extreme acceleration events can be observed in our DNS. As the most extreme of these events are relatively rare, typically not more than 1-3 counts in the histogram calculation, these extreme points of the PDFs are obviously and unavoidably not well-converged. Moreover, these extreme events will highly influence the kurtosis and make it difficult to observe a clear trend with the rotation rate. In the computation of the kurtosis we therefore only include acceleration events that occur with a probability  $P_{a_i} > 10^{-4}$  in the PDFs.

In figure 4a, we show  $K_{xy}$  and  $K_z$  for both the center and top measurement volumes in the convection cell (for the location, again, see figure 1). The values of the kurtosis measured in the DNS are in general more extreme than those measured experimentally in [18], where the difference can go up by a factor of four for both  $K_z$  and  $K_{xy}$  near the top plate and a factor of two in the center. This is a consequence of the extreme acceleration events in some (small-scale) vortex structures measured in the DNS which are washed out in the experimental data. Indeed, similar

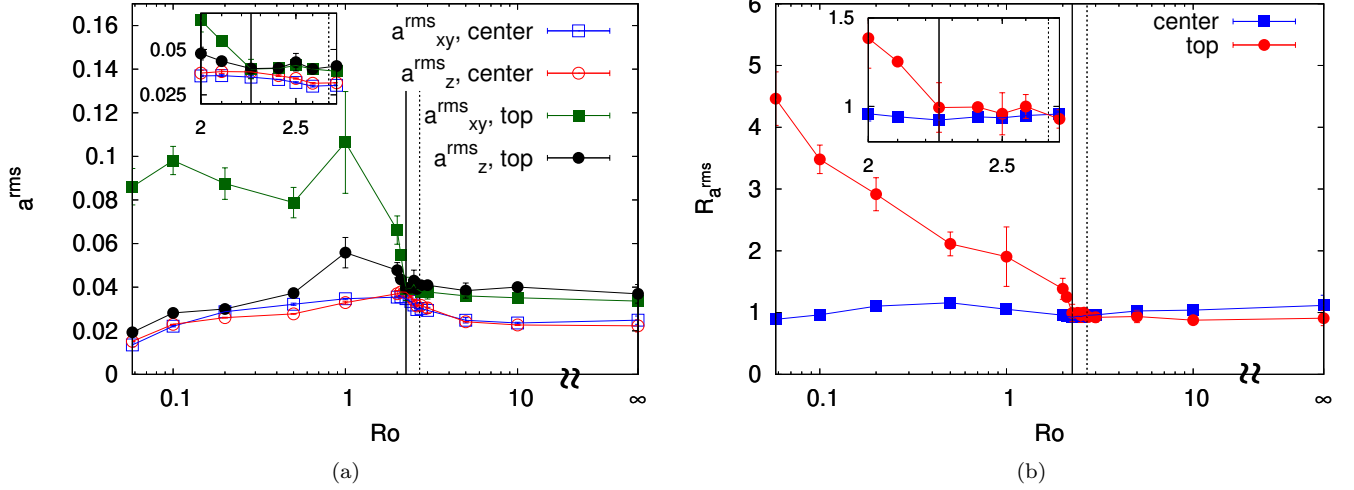


Figure 3: (a) Root-mean-square (rms) values of the horizontal and vertical acceleration components,  $a_{xy}^{rms}$  and  $a_z^{rms}$ , respectively, as a function of  $Ro$ . Statistics are collected in the center (open symbols) and near the top plate (closed symbols). (b) The ratio between the rms values of the horizontal and vertical acceleration components,  $R_a^{rms} = a_{xy}^{rms} / a_z^{rms}$ , for the center (blue crosses) and the top (red asterisks). In both panels the inset shows a zoom of the data in the range  $2 \leq Ro \leq 2.75$  and the vertical solid line represents  $Ro_{c2} = 2.25$ , the second critical Rossby number, clearly different from  $Ro_{c1} = 2.7$  (shown as the dotted line). Some of the error bars have the same size as the symbols, or are even smaller, and therefore not visible (the error bars are based on the differences between the results from the Lagrangian data obtained in the top and bottom half of the convection cell).

events are difficult to capture in the experiments where tracers always have a nonvanishing response time and where sudden movements of particles often results in losing these particles in the experimental particle-tracking procedure. Although the values do not match one-to-one with those measured in [18], the trend with rotation in the kurtosis is quite similar. Like in [18], the kurtosis is only weakly affected by rotation in the center, where  $K_{xy}$  has a local minimum around  $Ro \approx 0.5$ . This means that the PDFs of  $a_{xy}$  are more intermittent for very small and very large Rossby numbers in the center, which is a result of the presence of coherent flow structures, which dominate the flow in the small and large  $Ro$ -number regimes (vertically-aligned vortices versus the LSC). Near the top plate both  $K_{xy}$  and  $K_z$  suddenly increase at  $Ro_{c2} \approx 2.25$  to reach their maximum value at  $Ro \approx 2$ , and decreasing again for  $Ro \lesssim 2$ . The quantitative values differ significantly from what has been found in the experiments by [18], although the trends as a function of  $Ro$  are similar. With regard to these experimental data, this finding can be explained, on top of what has already been mentioned above with regard to the tracking algorithm, by the lack of (Lagrangian) data points inside the BL at the top plate in the experiments due to (i) a gap of about 1 mm between the top plate and the measurement volume and (ii) particles begin slightly heavier than the surrounding fluid (see also Ref. [52]). This BL is exactly the region where the thermal plumes develop that strongly accelerate the fluid horizontally (in the swirling plumes) and vertically away from the plate. In the experiments part of these extreme acceleration events near the top BL are thus missed, in particular the extreme vertical acceleration events in the swirling plumes. Since in the DNS the BL is fully included in the top measurement volume, extremal values of  $a_z$  and  $a_{xy}$  are included and hence extremal values of  $K_z$  and  $K_{xy}$  in the top measurement volume are obtained, compared to those from the experiments. All together, as in figure 3, the transition in the kurtosis observed near the top plate is very sudden and occurs at  $Ro_{c2} \approx 2.25$ .

The skewness, computed as  $S_i = \langle (a_i - \langle a_i \rangle)^3 \rangle / \langle (a_i - \langle a_i \rangle)^2 \rangle^{3/2}$ , gives a measure for the symmetry of the acceleration statistics. In figure 4b, we show  $S_{xy}$  and  $S_z$  as a function of  $Ro$  for both the center and the top measurement volumes, where we only include acceleration events with a probability  $P_{a_i} > 10^{-4}$  as we did for the kurtosis. In homogeneous isotropic turbulence (HIT), acceleration PDFs are symmetric and ideally  $S_i = 0$ . In the center, where the flow is closest to HIT [13, 32, 53], both  $S_{xy}$  and  $S_z$  indeed fluctuate around zero. Near the top plate,  $S_{xy}$  fluctuates around zero, but  $S_z < 0$ , i.e., PDFs of  $a_z$  are negatively skewed for all rotation rates. Plumes emerging from the BLs are accelerating the fluid moving away from the plates towards the bulk [31], resulting in more extreme negative acceleration events at the top plate. For  $Ro \lesssim 2.5$  these plumes progressively become of the Ekman type and at  $Ro_{c2} \approx 2.25$ ,  $S_z$  suddenly decreases (gets a more negative value, see figure 4b) to reach a minimum at  $Ro \approx 1$  to then increases again (thus getting a less negative value) for  $Ro \lesssim 1$ , similar to the trend in the kurtosis that displays an extremum in the range  $1 \lesssim Ro \lesssim 2$ .

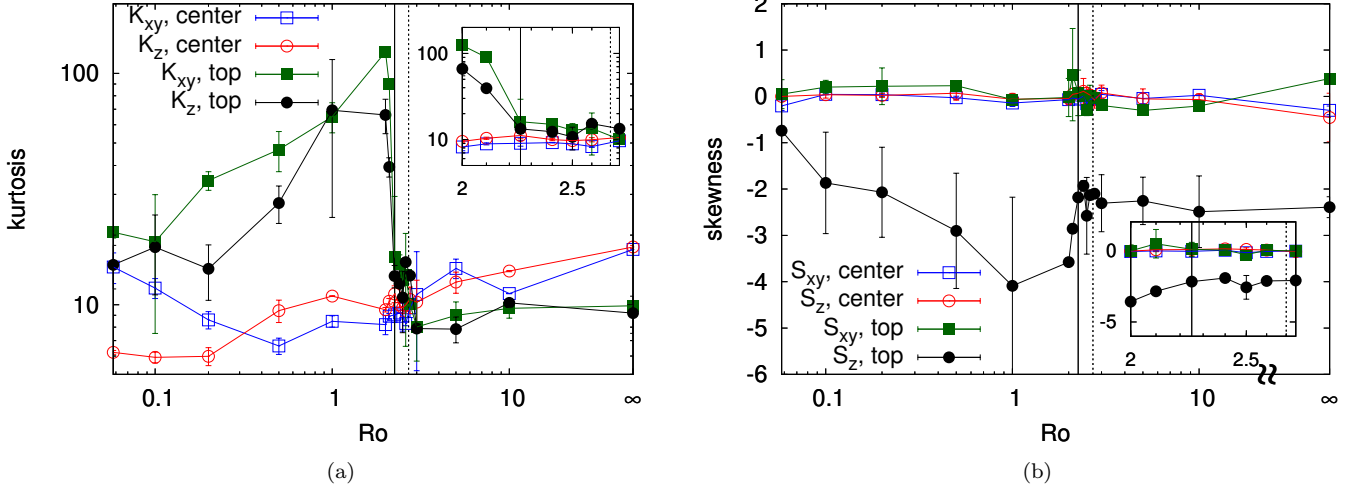


Figure 4: (a) Kurtosis and (b) skewness of the horizontal (squares) and vertical (circles) acceleration statistics as a function of  $Ro$ . Statistics are collected in the center (open symbols) and near the top plate (closed symbols). In both panels the inset shows a zoom of the data in the range  $2 \leq Ro \leq 2.75$ . The vertical solid line represents  $Ro_{c_2} = 2.25$ , and the vertical dotted line  $Ro_{c_1} = 2.7$ . Some of the error bars have the same size as the symbols, or are even smaller, and therefore not very well visible (the error bars are based on the differences between the results from the Lagrangian data obtained in the top and bottom half of the convection cell).

The rms values, kurtosis and skewness of the Lagrangian acceleration statistics near the top plate all show a distinct transition at  $Ro_{c_2} \approx 2.25$ . This critical Rossby number is smaller than the Rossby number at which the behavior of the Nusselt number shows a clear transition, for our particular parameter settings at  $Ro_{c_1} \approx 2.7$  as seen in figure 2, thus  $Ro_{c_2} < Ro_{c_1}$ . By decreasing the Rossby number beyond  $Ro_{c_2}$ , the three quantities  $a^{rms}$ ,  $K$  and  $S$  suddenly take very extreme values to then attenuate again for even lower  $Ro$ . This clearly suggests that there is also a sudden transition in the flow structures near the top plate at  $Ro_{c_2} \approx 2.25$ , which is possibly due to the transition from sheet-like thermal plumes in the Prandtl–Blasius type BL to vortical plumes emerging from the Ekman type BL.

### C. Root-mean-square values of acceleration in horizontal slabs

So far, we have distinguished the center and top measurement volumes as sketched in figure 1. We have found a sudden transition in the Lagrangian acceleration statistics at  $Ro_{c_2} \approx 2.25$  near the top plate, while in the center such a transition is absent. Since the measurement volume near the top plate spans a height of  $\Delta z = 0.05H$ , it is not clear at which  $z$ -position the signatures of the transition become visible. We are therefore also not able yet to pinpoint the physical mechanisms responsible for this transition. To investigate the transition more locally,  $a_i^{rms}$  is computed in horizontal slabs of thickness  $\Delta_{z_i} = 0.001H$  centered at different vertical positions  $z_i$ . In the bulk, statistics are computed for  $z_i/H = 0.5$ ,  $z_i/H = 0.8$  and  $z_i/H = 0.9$  (this latter value is most likely representing data in the bulk-BL mixed region). Near the BLs we take into account that the viscous BL thickness  $\delta_\nu$  varies with the rotation rate and we express  $z_i$  in terms of  $\delta_\nu$ . In figure 5 the normalized BL thickness  $\delta_\nu/H$  is shown as a function of  $Ro$ , computed from the current DNS as the position of the maximum of the horizontal rms velocity. Acceleration statistics are now computed in slabs with thickness  $\Delta_{z_i} = 0.001H$  centered around  $z_i = H - n\delta_\nu$ , with  $n \in \{2, \frac{3}{2}, \frac{1}{2}, \frac{1}{3}\}$ . The results for  $a_{xy}^{rms}$  and  $a_z^{rms}$  are normalized by its value for  $Ro = \infty$  in the corresponding slab, such that all curves have value unity at  $Ro = \infty$  as shown in figure 6. We see that the data for both  $a_{xy}^{rms}$  and  $a_z^{rms}$  almost overlap when  $Ro \gtrsim 2.25$ , while at  $Ro_{c_2} \approx 2.25$  the trend suddenly changes. Values of  $a_{xy}^{rms}$  start to increase with increasing rotation rate when  $z_i/H \gtrsim 0.9$  and  $Ro \lesssim 2.25$ , see figure 6a. For comparison, the viscous BL thickness for  $Ro > Ro_{c_2}$  is approximately constant and equals  $\delta_\nu/H \approx 0.032$  (see figure 5) such that the BL at the top plate start at  $z \approx 0.968H$  in this regime. For  $Ro < Ro_{c_2}$  the BL thickness decreases up to a value of  $\delta_\nu \approx 0.006H$  when  $Ro = 0.058$  (see figure 5) and the BL at the top plate starts at  $z \approx 0.994H$  for this rotation. Since the transition in  $a_{xy}^{rms}$  is already visible from  $z_i/H = 0.9$  on (a vertical position that is outside the viscous BL for all rotation rates), we can argue that Ekman plumes with a swirling horizontal motion emerge when  $Ro < Ro_{c_2}$  are also felt outside the BL (up to a distance of at least  $4\delta_\nu$  from the top plate).



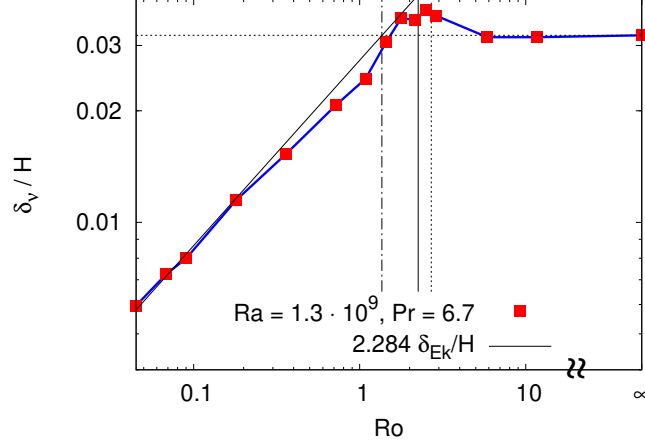


Figure 5: The viscous BL thickness  $\delta_\nu/H$  for cylindrical Rayleigh–Bénard convection with  $Ra = 1.3 \times 10^9$ ,  $Pr = 6.7$  and  $\Gamma = 1$ . The BL thickness is measured from the DNS as the position of the maximum of the horizontal rms velocity. The horizontal dashed line shows the kinetic BL thickness  $\delta_\nu/H = 0.032$  and the sloping solid black line shows the theoretical prediction based on the linear Ekman BL theory, where  $\delta_{Ek} = \sqrt{\nu/\Omega}$ , see [18]. The black dashed-dotted vertical line indicates the Rossby number where the viscous and Ekman BLs intersect ( $Ro \approx 1.4$ ). The vertical solid and dotted lines indicate  $Ro_{c2}$  and  $Ro_{c1}$ , respectively.

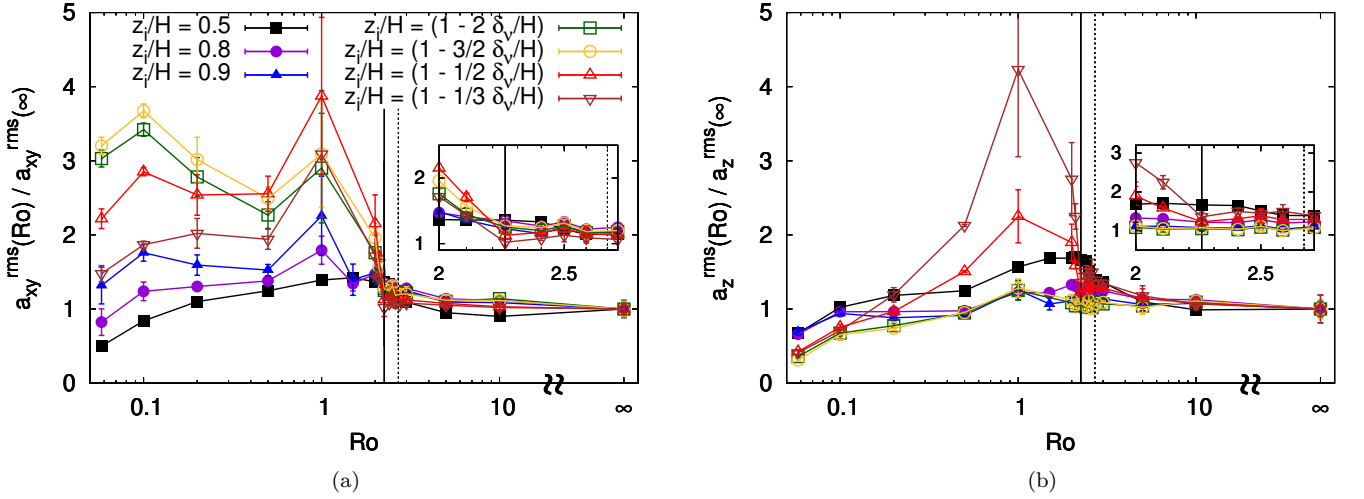


Figure 6: Rms values of the (a) horizontal and (b) vertical acceleration components, both normalized by the respective rms acceleration values of the non-rotating case,  $a_{xy}^{rms}(Ro)/a_{xy}^{rms}(\infty)$  and  $a_z^{rms}(Ro)/a_z^{rms}(\infty)$ , respectively. Rms values are computed in horizontal slabs of thickness  $\Delta_{z_i} = 0.001H$  and central position  $z_i$  as a function of  $Ro$ . The legend in panel (b) is the same as in panel (a) and in both panels the inset shows a zoom of the data in the range  $2 \leq Ro \leq 2.75$ . The vertical solid and dotted lines represent  $Ro_{c2} = 2.25$  and  $Ro_{c1} = 2.7$ , respectively.

While  $a_z^{rms}$  is only showing a weak increase at  $Ro_{c2}$  in the top measurement volume, see figure 3, a much stronger increase is observed in figure 6b for  $z_i/H \gtrsim 1 - \delta_\nu/H$  (brown and red curves in figure 6b), i.e., when statistics are collected inside the viscous BL. This indicates that rotation enhances the fluctuations in the vertical acceleration components only inside the BL, while it does not significantly affect these fluctuations inside the bulk. Since the BL is not turbulent in the parameter regime simulated here, this is expected to be purely related to the emergence of vortical plumes in the Ekman BL, accelerating the fluid away from the plate.

All together, figure 6 once again shows a sudden transition in the Lagrangian acceleration statistics at  $Ro_{c2} \approx 2.25$  close to the top plate, where the magnitude of the increase of the rms-values at this transition depends on  $z_i$ .

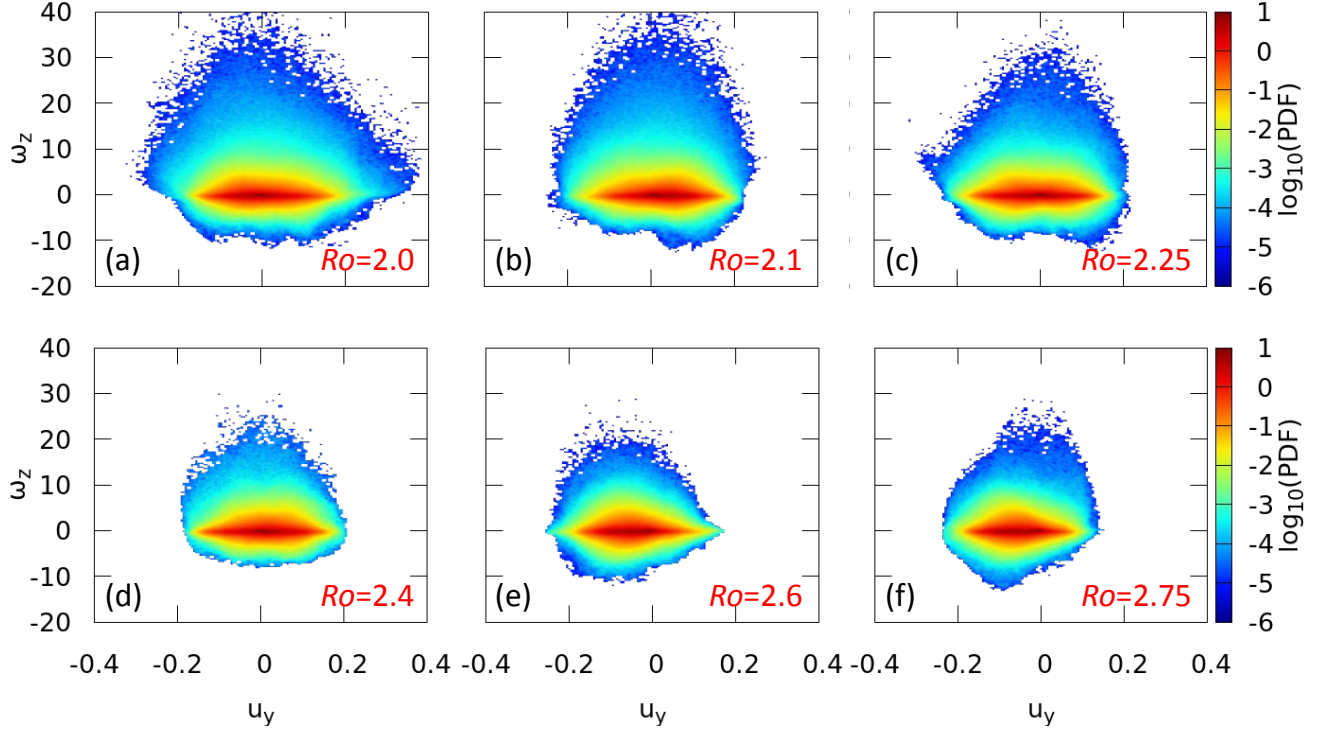


Figure 7: Joint PDFs of the horizontal Lagrangian velocity of passive tracers,  $u_y$ , and the vertical vorticity,  $\omega_z$ , measured in the top measurement volume for six different Rossby numbers.

#### D. Flow structures near the top plate

To understand why the Lagrangian acceleration statistics show such an extreme transition at  $Ro_{c_2} \approx 2.25$ , and why it occurs at a smaller Rossby number than the transition in the behavior of the (normalized) Nusselt number ( $Ro_{c_2} < Ro_{c_1}$ ), we need to better understand the underlying flow structures. For this purpose, we will consider joint PDFs of the vertical vorticity  $\omega_z$  (obtained from the Eulerian flow field) with (i) the horizontal and vertical Lagrangian velocities  $u_y$  and  $u_z$ , respectively, and (ii) the horizontal Lagrangian acceleration  $a_{xy}$ . Note that we do not use the horizontally-averaged  $u_{xy}$ , as we do for the acceleration statistics, because with the separate horizontal velocity components we can better distinguish the presence of the LSC. With the joint PDFs of vertical vorticity and horizontal velocity we can potentially provide some insight into the fate of the large-scale circulation (LSC) with decreasing  $Ro$ . On the other hand, the joint PDFs of vertical vorticity with the vertical component of velocity and horizontal components of acceleration are suitable to potentially visualize the formation of vertically-aligned vortical structures when approaching  $Ro_{c_2}$ . To improve the statistics we now use a slightly larger measurement volume of size  $0.4H \times 0.4H \times 0.25H$ , starting at  $z = 0.75H$  and ending at  $z = H$ , i.e., reaching all the way to the top plate.

In figure 7 we have plotted the joint PDFs of the horizontal Lagrangian velocity component,  $u_y$ , and the vertical vorticity  $\omega_z$  for  $Ro \in \{2.0, 2.1, 2.25, 2.4, 2.6, 2.75\}$ . For the highest Rossby numbers we clearly see the remnants of the LSC as the maximum of the joint PDFs have negative  $u_y$  and an almost symmetric vertical vorticity distribution (provided the joint probability  $P_{joint} \gtrsim 10^{-3}$ ). A lack of symmetry in the vorticity distribution occurs for high positive vorticity values (with rather low probability) and is due to the emergence of weak cyclonic vortices near the top plate, while the (remnants of the) LSC are still dominant (see also discussion below). Similar joint PDFs with  $u_x$  show a maximum with  $u_x > 0$ . For  $Ro = 2.4$  the maximum of the joint PDF has moved to the origin  $(u_y, \omega_z) = (0, 0)$  and the vorticity distribution becomes asymmetric with a strong preference for positive vertical vorticity, indicating emergence of cyclonic vortices. These cyclonic vortices become stronger with decreasing  $Ro$ . For  $Ro \lesssim 2.25$  the  $\omega_z$ -distribution becomes even more asymmetric and the  $u_y$  are basically symmetrically distributed around  $u_y = 0$  (with predominantly positive  $\omega_z$ ). This is a clear signature of the dominance of vertically-aligned cyclonic vortices which must possess the same amount of positive and negative  $u_y$  (pure swirling flows in the vortex cores). The destruction of the LSC and formation of vertically-aligned cyclonic vortices is nicely confirmed by the joint PDFs of the vertical Lagrangian velocity component  $u_z$  and the vertical vorticity  $\omega_z$  for the same range of  $Ro$ , see figure 8. Particularly

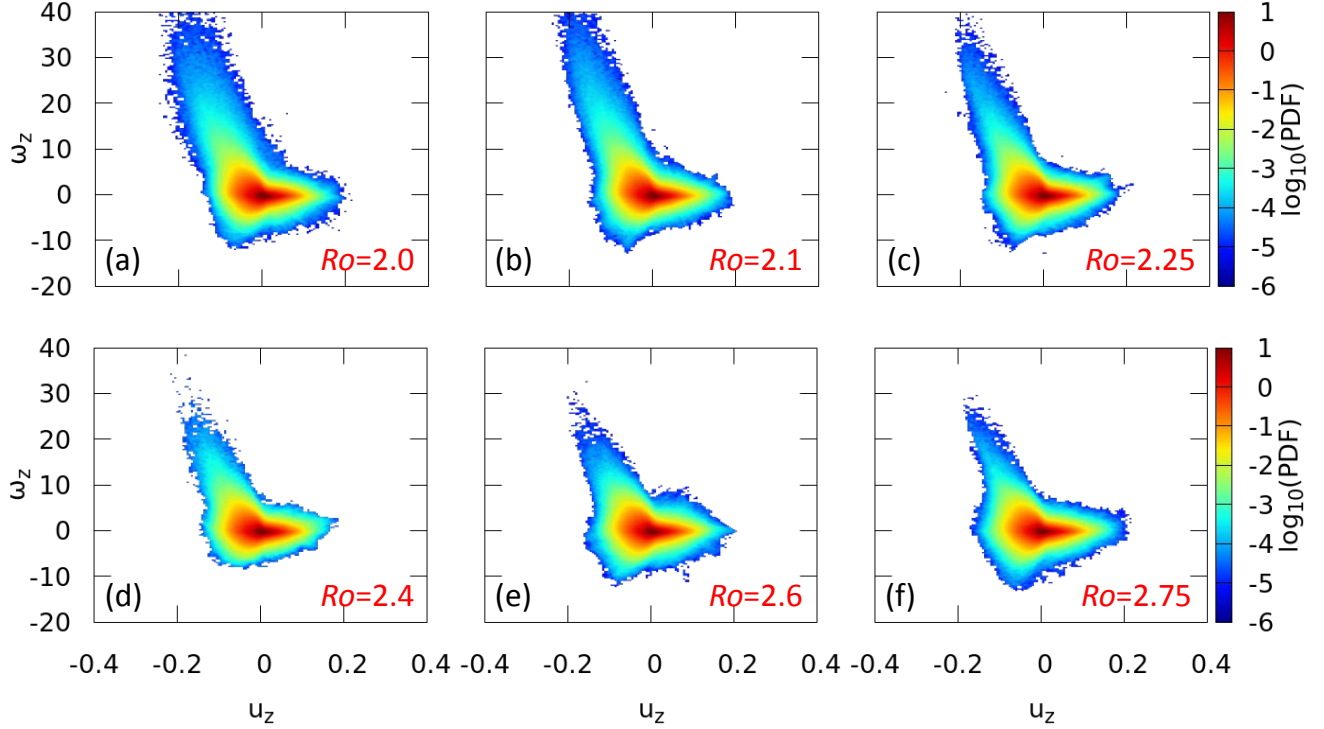


Figure 8: Joint PDFs of the vertical Lagrangian velocity of passive tracers,  $u_z$ , and the vertical vorticity,  $\omega_z$ , measured in the top measurement volume for six different Rossby numbers.

convincing is the strong correlation of positive vertical vorticity with negative vertical velocity for  $Ro \lesssim 2.25$ . Quite remarkably, a correlation between positive  $\omega_z$  and negative  $u_z$  is already visible for  $Ro \gtrsim 2.4$  which suggests that weak cyclonic vortices are already being formed near the top plate while the LSC is being weakened (see figure 7). These aspects can be confirmed and explored further with the joint PDFs of vertical vorticity and horizontal acceleration of passive tracers.

It is expected that the thermal plumes developing in the BLs at the horizontal plates are responsible for the extreme horizontal and vertical acceleration of fluid parcels. For  $Ro \gtrsim 2.25$  the results presented and discussed in the previous (sub)sections suggest that these should predominantly be sheet-like thermal plumes and the LSC (or large-scale remnants of it) induces a mean wind at the horizontal plates as confirmed by the joint PDFs of vertical vorticity and horizontal velocity above, deflecting the plumes into the direction of the mean horizontal flow [54]. Thermal plumes in the Prandtl–Blasius BL are characterized by large values of both positive and negative vertical vorticity, while vortical plumes emerging from the Ekman BL are cyclonic, i.e. they spin up in the same direction as the applied rotation  $\Omega$ , resulting in positive vertical vorticity [33, 36], with extreme values of  $\omega_z$ . In the regime unaffected or weakly affected by rotation the deflection of the plumes by the mean wind is expected to largely suppress and flush away emerging regions of extreme vertical vorticity. The LSC has become already much weaker for  $Ro \lesssim Ro_{c_2} \approx 2.25$  [10, 15, 35, 55] (see also figure 7 and Table I) and in this regime regions with large and extreme positive vertical vorticity are expected to be much more dominant and persistent. Therefore, in this rotation-affected regime we do expect the extreme (horizontal) acceleration of tracers to be much more clearly correlated to the swirling motion of vortical plumes.

Vortical plumes in the Ekman BL spin up cyclonically and we thus expect extreme acceleration events to occur in regions with positive vertical vorticity. To investigate this relation between acceleration and vorticity, we compute the joint PDFs of the horizontal acceleration  $a_{xy}$ , and the vertical vorticity  $\omega_z$ . Results of these joint PDFs are shown in figure 9 for six different Rossby numbers around the transition at  $Ro_{c_2} \approx 2.25$ . Although the behavior of the joint PDFs around this transition appears to be more gradual, a different behavior is clearly found before and after the transition at  $Ro_{c_2}$ . When  $Ro \gtrsim 2.4$ , the joint PDFs show an elongated patch centered in the origin ( $\omega_z = 0$ ,  $a_{xy} = 0$ ), and the most abundant acceleration events, that occur with a probability  $P_{joint} > 10^{-4}$ , are almost symmetrically distributed with respect to  $\omega_z = 0$  (see the area from red to light blue in the scatter plots; the dark blue area contributes less strongly as there  $10^{-7} \lesssim P_{joint} \lesssim 10^{-4}$ ), indicating that acceleration events are correlated to small positive and negative values of  $\omega_z$ . When  $Ro \lesssim 2.4$ , values of  $\omega_z$  and  $a_{xy}$  have become more

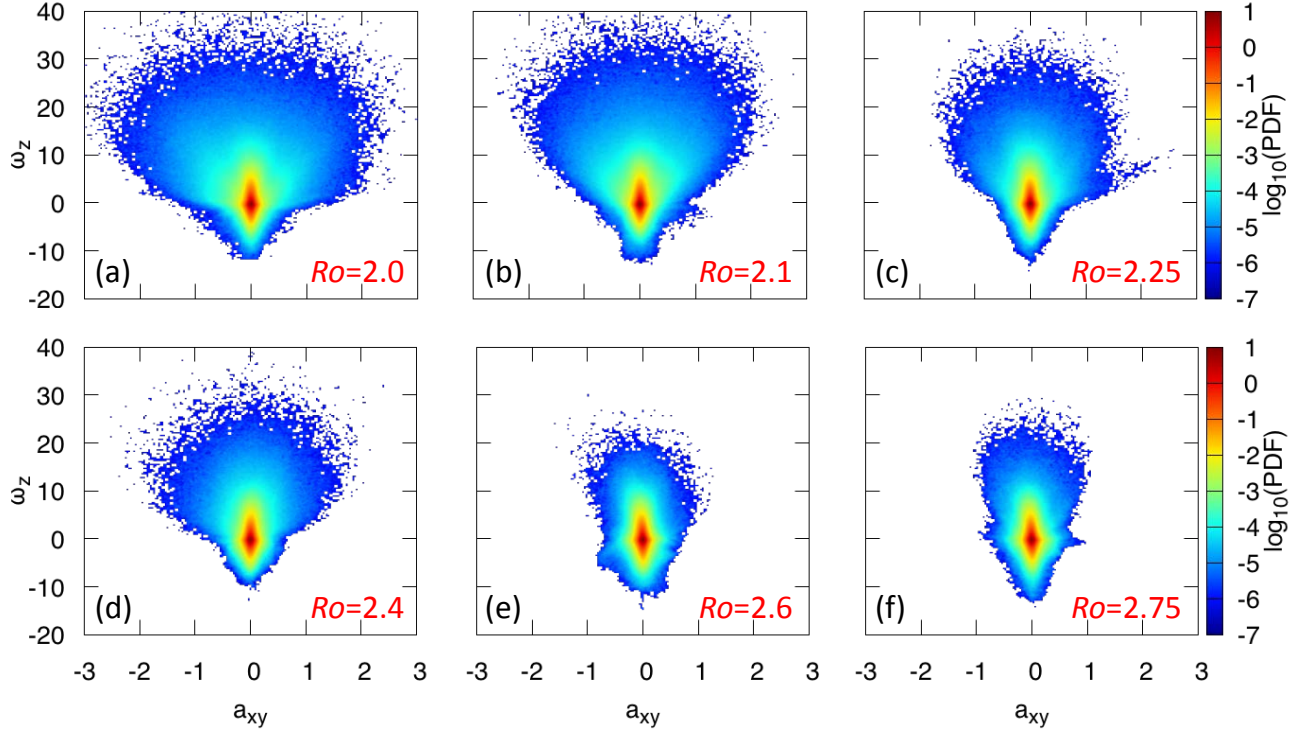


Figure 9: Joint PDFs of the horizontal Lagrangian acceleration of passive tracers,  $a_{xy}$ , and the vertical vorticity,  $\omega_z$ , measured in the top measurement volume for six different Rossby numbers.

extreme (see the extension of the dark blue area) and now larger acceleration events, indicated by the red to light blue areas in the joint PDFs (with the joint probability  $P_{joint} > 10^{-4}$ ), are correlated to large values of mostly positive  $\omega_z$ . The acceleration events that occur with a joint probability  $P_{joint} > 10^{-4}$  are thus asymmetrically distributed around  $\omega_z = 0$ . Although signatures of the transition are already visible for  $Ro \approx 2.4$ , in particular for the extreme acceleration events, the observations suggest that tracers exposed to large accelerations are trapped inside Ekman plumes with cyclonic vorticity, most clearly for  $Ro \lesssim Ro_{c2}$ .

#### IV. CONCLUSIONS

We have investigated the effect of rotation on the Lagrangian acceleration statistics of passive tracers in RBC, where the focus is on the drastic change in the flow structures around the transition in heat transfer efficiency when going from the rotation-unaffected to the rotation-affected regime. The horizontal acceleration statistics near the top plate show a sudden transition at  $Ro_{c2} \approx 2.25$ , below which the rms values and the kurtosis increase significantly. When collecting statistics in thin horizontal slabs at different vertical positions  $z_i$ , relative to the BL thickness, we find that the transition in the flow structures can be observed up to  $z_i/H \gtrsim 0.9$ , thus in the turbulent bulk quite far outside the boundary layer itself. Although rms values of vertical acceleration collected in the measurement volume near the top plate do not show a drastic transition at  $Ro_{c2}$ , a sudden increase is found when measuring rms values of vertical acceleration inside the viscous BL. This is a Lagrangian signature of the presence of Ekman plumes strongly accelerating the fluid horizontally spiraling inwards into vertically-aligned vortices before being injected into the bulk. The kurtosis and skewness of  $a_z$  do show a sharp transition in the top measurement volume.

Since transitions in the Lagrangian acceleration statistics are only found close to the top plate and not in the center of the cell, they are expected to be related to the development of thermal plumes in the BLs at the plates. Under rotation, these thermal plumes change from sheet-like plumes in the Prandtl-Blasius type BL regime to vertically-aligned vortical plumes in the Ekman type BL regime. To investigate the relation between the Lagrangian acceleration of fluid particles (or passive tracers) and the thermal plumes, we focused on the joint statistics of horizontal and vertical Lagrangian velocity components  $u_y$  and  $u_z$ , respectively, with the vertical vorticity  $\omega_z$  and on those of  $a_{xy}$  and the vertical vorticity  $\omega_z$ . In the rotation-unaffected regime, joint PDFs of  $a_{xy}$  and  $\omega_z$  are symmetric around  $\omega_z = 0$  and do not show significant extreme acceleration events when  $Ro \gtrsim Ro_{c2}$ . This behavior completely changes when moving

into the rotation-affected regime, in particular for  $Ro \lesssim Ro_{c_2}$ , where joint PDFs show a clear correlation between strong horizontal acceleration events and positive values of  $\omega_z$ . At the transition  $Ro_{c_2}$ , also the maximum values of  $\omega_z$  increase drastically together with the emergence of extreme horizontal acceleration events. This suggests that the coherent structures in and near the Ekman BL are rather suddenly dominated by strong vertically-aligned vortical structures.

This conclusion is supported by the joint PDFs of horizontal and vertical Lagrangian velocity with vertical vorticity, see figures 7 and 8. These PDFs indeed confirm the notion that the LSC does not disappear suddenly at  $Ro_{c_1}$ , but is slowly being destroyed. The remnants of the LSC are still able to sweep away emerging cyclonic vortices near the plates (which obviously tend to emerge for  $Ro \gtrsim 2.4$ , see figure 8). This is in agreement with observations in Ref. [10] where it was concluded (with numerical simulations for  $Ra = 1.0 \times 10^9$  and  $Pr = 6.4$ ) that the LSC becomes weaker for  $Ro \lesssim 2.5$ , but significant amounts of energy are still stored in the LSC motion down to  $Ro \approx 1.2$ , although rapidly decreasing with  $Ro$ . Experimental data on the properties of the LSC for  $Ra = 2.25 \times 10^9$  and  $Pr = 4.38$  reveal a similar picture, see [15]. See also [35] where a different measure is applied for the LSC strength and an extended dataset from [15] is used for comparison. These experimental data clearly reveal that the LSC strength is significantly decreased when Rossby is reduced to  $Ro \approx 1.2$ . Also in Ref. [13] it was observed that slightly enhanced values of horizontal and vertical root-mean-square velocities remain quite constant down to  $Ro \approx 1.2$ .

In previous experiments [18] we were already able to use Lagrangian acceleration statistics to explore the transition. However, within the resolution of Rossby numbers used in that study the transition seemed gradual and, if present, it could still be connected with the known critical rotation rate for heat transfer enhancement (here indicated with  $Ro_{c_1}$ ). In the present study we indeed see a sudden sharp transition in the Lagrangian acceleration statistics at  $Ro_{c_2} \approx 2.25$ . However, this critical Rossby number turns out to be *smaller* than  $Ro_{c_1} \approx 2.7$ . Thus at both rotation rates sharp transitions are observed, but for different quantities. By looking at the acceleration of tracers and its relation to typical plume characteristics, we found that Ekman plumes are much more efficient in accelerating fluid parcels causing this sudden transition in the Lagrangian acceleration statistics.

The most remarkable observation of this study is not the sharpness of the transition in the Lagrangian acceleration statistics, but the presence of two critical Rossby numbers while only one was anticipated in advance: (i) the well-known critical Rossby number  $Ro_{c_1}$ , indicating a sudden and sharp transition in heat transport properties in rotating RBC, and (ii) a new critical Rossby number  $Ro_{c_2} < Ro_{c_1}$  where the Lagrangian acceleration statistics show a sharp transition. The latter is intimately related with a change in dominant flow structures, i.e. from LSC to vertically-aligned vortices, which does not occur at  $Ro_{c_1}$  but at  $Ro_{c_2}$ . Intuitively, one would expect that  $Ro_{c_2} = Ro_{c_1}$  which is clearly not the case. The present observations hint at two BL related mechanisms responsible for these transitions and with which we can derive crude estimates for both Rossby numbers at which the transitions can take place.

In figure 5 we have indicated the Rossby number at which the Ekman type BL and the viscous Prandtl-Blasius type BL have similar thickness. It was based on the assumption  $2.284\delta_{Ek} = \delta_\nu$  (see the next paragraph for a brief motivation), or put slightly differently:  $\delta_{Ek}/H = \sqrt{2Ro(Pr/Ra)^{1/2}} = \delta_\nu/(2.284H)$ . We can rewrite this as

$$Ro = \frac{1}{2} \left( \frac{\delta_\nu}{2.284H} \right)^2 \sqrt{\frac{Ra}{Pr}}. \quad (4)$$

The dimensionless BL thickness in our non-rotating RBC case (with  $Ra = 1.3 \times 10^9$ ,  $Pr = 6.7$  and  $\Gamma = 1$ ) is  $\delta_\nu/H \approx 0.032$ , see figure 5. From Eq. (4), the required Rossby number to satisfy  $2.284\delta_{Ek} = \delta_\nu$  is then  $Ro_{c_2,th} \approx 1.4$ , somewhat smaller than  $Ro_{c_2} \approx 2.25$ , but consistent with Rossby-number estimates for the disappearance of the LSC [10, 15, 35].

The first critical Rossby number,  $Ro_{c_1} \approx 2.7$ , reflects the rotation rate where  $\frac{\partial \mathbf{u}_h}{\partial z}|_{z=0}$ , with  $\mathbf{u}_h = (u, v)$  in the Ekman type BL, becomes similar in magnitude to the normal gradient of the horizontal velocity component in the Prandtl-Blasius type BL at the wall. Note that under this condition the Ekman type BL thickness is then larger than the thickness of the Prandtl-Blasius type BL.

To estimate the Rossby number for this to occur we compare the Ekman type BL with an approximation for the BL over the flat bottom and top plates in non-rotating RBC, the Blasius BL. The starting point is the fact that for similar thicknesses of these BLs the normal gradient at the plate is larger in magnitude for the Ekman BL compared to this gradient for the Blasius BL [56]. Using linear Ekman boundary-layer theory, see [57], the matching of a geostrophic bulk flow with velocity  $V$  (which we assume for convenience to be in the  $x$ -direction) to the solid wall gives the following expressions for the horizontal velocity field in the Ekman boundary layer:  $u = V[1 - e^{-z/\delta_{Ek}} \cos(z/\delta_{Ek})]$  and  $v = V e^{-z/\delta_{Ek}} \sin(z/\delta_{Ek})$ . This immediately results in  $\frac{\partial u}{\partial z}|_{z=0} = V/\delta_{Ek}$  and similarly for  $\frac{\partial v}{\partial z}|_{z=0}$  (and the maximum of  $\sqrt{u^2 + v^2} \approx 1.07V$  at  $z = 2.284\delta_{Ek}$ , which we consider as the actual Ekman BL thickness and which is used as such in figure 5, before asymptotically reducing to  $V$  for large  $z$ ). Using the well-known properties of the Blasius BL that  $\frac{\partial u}{\partial z}|_{z=0} = 0.33$  and  $\tilde{\delta}_\nu = 4.9$  (in the non-dimensional BL units and the  $u = 0.99V$  criterion for  $\delta_\nu$  [56]), we find here that  $\frac{\partial u}{\partial z}|_{z=0} = 0.33 \cdot 4.9 \frac{V}{\delta_\nu} \approx 1.62 \frac{V}{\delta_\nu}$ . To obtain a similar magnitude of the normal velocity gradient at the plate

for the two cases, we should consider an Ekman BL that is approximately 41% thicker than the Blasius BL thickness, thus we should have an Ekman BL thickness  $2.284\delta_{Ek} \approx 1.41\delta_\nu$ . Substituting this approximate equality into Eq. (4), yields an enhanced value of  $Ro$  by a factor  $1.41^2$ , thus  $Ro_{c1,th} \approx 2.8$ , which is very close to  $Ro_{c1} \approx 2.7$ .

When  $Ro \gtrsim 2.8$  the normal velocity gradient at the wall is determined by the Prandtl-Blasius BL and remains more or less constant (and  $Nu$  will not change drastically by changing the rotation rate). For sufficiently high rotation rates such that  $Ro \lesssim 2.8$ , we expect that the mean velocity gradient in the BL will progressively steepen with increasing rotation rate as the Ekman BL thickness decreases proportional to  $1/\sqrt{\Omega}$ . The thermal BL is fully embedded within the viscous BL and in case the latter gets thinner the thermal BL is increasingly exposed to larger average tangential velocities resulting in an increased normal temperature gradient at the plate. We expect that as a consequence also the thickness  $\delta_T$  of the thermal BL must become somewhat thinner, see, for example, Ref. [13]. The Nusselt number, defined as  $Nu = \frac{H}{2\lambda_T}$ , should increase as heat will be released more efficiently to the (top) plate. Meanwhile, sheet-like thermal plumes will be formed at the plates and the rotation rate is not yet sufficiently strong to initiate a strong swirl in the converging flow at the base of the sheet-like thermal plume. At the second critical Rossby number ( $Ro_{c2}$ ), the rotation is strong enough to suddenly support a strong swirling flow towards the thermal plumes and simultaneously a strong vortical motion is set up in the suddenly emerging vertically-aligned vortex tubes. This interpretation is also supported by the joint PDFs of vertical vorticity and horizontal Lagrangian velocity as between both critical Rossby numbers a clear change in behavior from LSC-like flow to swirling flows near the top plate for decreasing Rossby number is observed. Although this scenario has to be analyzed in more detail, the main message is that the steepening of the velocity gradients at the wall and the generation of swirling converging flows in the BLs are two partially separate processes with different manifestations: (i) heat transfer enhancement at  $Ro_{c1}$  and (ii) sudden generation of vertically-aligned vortex tubes connecting BL to the bulk at  $Ro_{c2}$  and remarkably not at  $Ro_{c1}$ , in contrast to the common assumption in the literature.

In future research, it is of interest to study the link between both transitions in more detail by looking at, for example, the dissipation rate at different vertical positions around the transition. Since the strength of the thermal plumes is known to depend on the Prandtl number, studying the effect of rotation on Lagrangian acceleration statistics at different Prandtl numbers can give further insight into the plume dynamics in rotating RBC.

## ACKNOWLEDGMENTS

This work is financially supported by the Nederlandse Organisatie voor Wetenschappelijk Onderzoek I (NWO-I), the Netherlands. The authors gratefully acknowledge the support of NWO for the use of supercomputer facilities (Cartesius) under Grant No. 16289. R.P.J.K. has received funding from the H2020 European Research Council (ERC) under the European Union's Horizon 2020 research and innovation programme (grant number 678634). EU-COST action MP1305 "Flowing matter" is gratefully acknowledged.

- 
- [1] J.-C. Gascard, A.J. Watson, M.-J. Messias, K.A. Olsson, T. Johannessen, and K. Simonsen, Long-lived vortices as a mode of deep ventilation in the Greenland Sea, *Nature* **416**, 525 (2002).
  - [2] J. Marshall and F. Schott, Open-ocean convection: Observations, theory, and models, *Rev. Geophys.* **37**, 1 (1999).
  - [3] G. Hadley, Concerning the cause of the general trade-winds, *Phil. Trans.* **39**, 58 (1753).
  - [4] K.A. Emanuel, J.D. Neelin, and C.S. Bretherton, On largescale circulations in convecting atmospheres, *Q. J. Royal Meteorol. Soc.* **120**, 1111 (1994).
  - [5] G. Ahlers, S. Grossmann, and D. Lohse, Heat transfer and large scale dynamics in turbulent Rayleigh-Bénard convection, *Rev. Mod. Phys.* **81**, 503 (2009).
  - [6] D. Lohse and K.-Q. Xia, Small-scale properties of turbulent Rayleigh-Bénard convection, *Annu. Rev. Fluid Mech.* **42**, 335 (2010).
  - [7] F. Chilla and J. Schumacher, New perspectives in turbulent Rayleigh-Bénard convection, *Eur. J. Phys. E* **35**, 58 (2012).
  - [8] S.B. Pope, *Turbulent Flows* (Cambridge University Press, Cambridge, 2000).
  - [9] Y. Liu and R.E. Ecke, Heat transport scaling in turbulent Rayleigh-Bénard convection: Effects of rotation and Prandtl number, *Phys. Rev. Lett.* **79**, 2257 (1997).
  - [10] R.P.J. Kunnen, H.J.H. Clercx, and B.J. Geurts, Breakdown of large-scale circulation in turbulent rotating convection, *Europhys. Lett.* **84**, 24001 (2008).
  - [11] R.J.A.M. Stevens, J.-Q. Zhong, H.J.H. Clercx, G. Ahlers, and D. Lohse, Transitions between turbulent states in rotating Rayleigh-Bénard convection, *Phys. Rev. Lett.* **103**, 024503 (2009).
  - [12] J.-Q. Zhong, R.J.A.M. Stevens, H.J.H. Clercx, R. Verzicco, D. Lohse, and G. Ahlers, Prandtl-, Rayleigh-, and Rossby-number dependence of heat transport in turbulent rotating Rayleigh-Bénard convection, *Phys. Rev. Lett.* **102**, 044502 (2009).



- [13] R.P.J. Kunnen, B.J. Geurts, H.J.H. Clercx, Experimental and numerical investigation of turbulent convection in a rotating cylinder, *J. Fluid Mech.* **642**, 445 (2010).
- [14] S. Weiss, R.J.A.M. Stevens, J.-Q. Zhong, H.J.H. Clercx, D. Lohse, and G. Ahlers, Finite-size effects lead to supercritical bifurcations in turbulent rotating Rayleigh–Bénard convection, *Phys. Rev. Lett.* **105**, 224501 (2010).
- [15] J.-Q. Zhong and G. Ahlers, Heat transport and the large-scale circulation in rotating turbulent Rayleigh–Bénard convection, *J. Fluid Mech.* **665**, 300 (2010).
- [16] R.J.A.M. Stevens, J. Overkamp, D. Lohse, and H.J.H. Clercx, Effect of aspect ratio on vortex distribution and heat transfer in rotating Rayleigh–Bénard convection, *Phys. Rev. E* **84**, 056313 (2011).
- [17] P. Wei, S. Weiss, and G. Ahlers, Multiple transitions in rotating turbulent Rayleigh–Bénard convection, *Phys. Rev. Lett.* **114**, 114506 (2015).
- [18] H. Rajaei, P. Joshi, K.M.J. Alards, R.P.J. Kunnen, F. Toschi, and H.J.H. Clercx, Transitions in turbulent rotating convection: a Lagrangian perspective, *Phys. Rev. E* **93**, 043129 (2016).
- [19] K.L. Chong, Y. Yang, S.-D. Huang, J.-Q. Zhong, R.J.A.M. Stevens, R. Verzicco, D. Lohse, and K.-Q. Xia, Confined Rayleigh–Bénard, rotating Rayleigh–Bénard, and double diffusive convection: a unifying view on turbulent transport enhancement through coherent structure manipulation, *Phys. Rev. Lett.* **119**, 064501 (2017).
- [20] G.S. Lewis and H.L. Swinney, Velocity structure functions, scaling, and transitions in high-Reynolds-number Couette–Taylor flow, *Phys. Rev. E* **59**, 5457 (1999).
- [21] S. Grossmann, D. Lohse, and C. Sun, High-Reynolds number Taylor–Couette turbulence, *Annu. Rev. Fluid Mech.* **48**, 53 (2016).
- [22] F. Ravelet, L. Marié, A. Chiffaudel, and F. Daviaud, Multistability and memory effect in a highly turbulent flow: experimental evidence for a global bifurcation, *Phys. Rev. Lett.* **93**, 164501 (2004).
- [23] F. Ravelet, A. Chiffaudel, and F. Daviaud, Supercritical transition to turbulence in an inertially driven von Kármán closed flow, *J. Fluid Mech.* **601**, 339 (2008).
- [24] S.G. Huisman, R.C.A. van der Veen, C. Sun, and D. Lohse, Multiple states in highly turbulent Taylor–Couette flow, *Nat. Commun.* **5**, 3820 (2014).
- [25] R.P.J. Kunnen, H.J.H. Clercx, and B.J. Geurts, Heat flux intensification by vortical flow localization in rotating convection, *Phys. Rev. E* **74**, 056306 (2006).
- [26] H.T. Rossby, A study of Bénard convection with and without rotation, *J. Fluid Mech.* **36**, 309 (1969).
- [27] R.J.A.M. Stevens, H.J.H. Clercx, and D. Lohse, Optimal Prandtl number for heat transfer in rotating Rayleigh–Bénard convection, *New J. Phys.* **12**, 075005 (2010).
- [28] P. Vorobieff and R.E. Ecke, Vortex structure in rotating Rayleigh–Bénard convection, *Physica D* **123**, 153 (1998).
- [29] R.P.J. Kunnen, R.J.A.M. Stevens, J. Overkamp, C. Sun, G.J.F. van Heijst, and H.J.H. Clercx, The role of Stewartson and Ekman layers in turbulent rotating Rayleigh–Bénard convection, *J. Fluid Mech.* **688**, 422 (2011).
- [30] R.J.A.M. Stevens, H.J.H. Clercx, and D. Lohse, Boundary layers in rotating weakly turbulent Rayleigh–Bénard convection, *Phys. Fluids* **22**, 085103 (2010).
- [31] K. Julien, S. Legg, J. McWilliams, and J. Werne, Hard turbulence in rotating Rayleigh–Bénard convection, *Phys. Rev. E* **53**, R5557 (1996).
- [32] H. Rajaei, P. Joshi, R.P.J. Kunnen, H.J.H. Clercx, Flow anisotropy in rotating buoyancy-driven turbulence, *Phys. Rev. Fluids* **1**, 044403 (2016).
- [33] K. Julien, S. Legg, J. McWilliams, and J. Werne, Rapidly rotating turbulent Rayleigh–Bénard convection, *J. Fluid Mech.* **322**, 243 (1996).
- [34] S. Stellmach, M. Lischper, K. Julien, G. Vasil, J.S. Cheng, A. Ribeiro, E.M. King, and J.M. Aurnou, Approaching the asymptotic regime of rapidly rotating convection: boundary layers versus interior dynamics, *Phys. Rev. Lett.* **113**, 254501 (2014).
- [35] R.J.A.M. Stevens, H.J.H. Clercx, and D. Lohse, Heat transport and flow structure in rotating Rayleigh–Bénard convection, *Eur. J. Mech. B/Fluids* **40**, 41-49 (2013).
- [36] O. Shishkina and C. Wagner, Analysis of sheet-like thermal plumes in turbulent Rayleigh–Bénard convection, *J. Fluid Mech.* **599**, 383 (2008).
- [37] E.M. King, S. Stellmach, and J.M. Aurnou, Heat transfer by rapidly rotating Rayleigh–Bénard convection, *J. Fluid Mech.* **691**, 568 (2012).
- [38] K. Julien, E. Knobloch, A.M. Rubio, and G.M. Vasil, Heat transport in low-Rossby-number Rayleigh–Bénard convection, *Phys. Rev. Lett.* **109**, 254503 (2012).
- [39] S. Horn and O. Shishkina, Rotating non-Oberbeck Boussinesq Rayleigh–Bénard convection in water, *Phys. Fluids* **26**, 055111 (2014).
- [40] R.E. Ecke and J.J. Niemela, Heat transport in the geostrophic regime of rotating Rayleigh–Bénard convection, *Phys. Rev. Lett.* **113**, 114301 (2014).
- [41] H. Rajaei, K.M.J. Alards, R.P.J. Kunnen, and H.J.H. Clercx, Velocity and acceleration statistics in rapidly rotating Rayleigh–Bénard convection, *J. Fluid Mech.* **857**, 374 (2018).
- [42] M.A. Green, C.W. Rowley, and G. Haller, Detection of Lagrangian coherent structures in three-dimensional turbulence, *J. Fluid Mech.* **572**, 111 (2007).
- [43] J. Schumacher, Lagrangian studies in convective turbulence, *Phys. Rev. E* **79**, 056301 (2009).
- [44] Y. Choi, Y. Park, and C. Lee, Helicity and geometric nature of particle trajectories in homogeneous isotropic turbulence, *Int. J. Heat Fluid Flow* **31**, 482 (2010).
- [45] L. Biferale, G. Boffetta, A. Celani, B.J. Devenish, A. Lanotte, and F. Toschi, Multifractal statistics of Lagrangian velocity

- and acceleration in turbulence, *Phys. Rev. Lett.* **93**, 064502 (2004).
- [46] F. Moisy and J. Jiménez, Geometry and clustering of intense structures in isotropic turbulence, *J. Fluid Mech.* **513**, 111 (2004).
  - [47] G.A. Voth, A. La Porta, A.M. Crawford, J. Alexander, and E. Bodenschatz, Measurement of particle accelerations in fully developed turbulence, *J. Fluid Mech.* **469**, 121 (2002).
  - [48] L. Del Castello and H.J.H. Clercx, Lagrangian acceleration of passive tracers in statistically steady rotating turbulence, *Phys. Rev. Lett.* **107**, 214502 (2011).
  - [49] R. Verzicco and R. Camussi, Numerical experiments on strongly turbulent thermal convection in a slender cylindrical cell, *J. Fluid Mech.* **477**, 19 (2003).
  - [50] R. Verzicco and P. Orlandi, A finite-difference scheme for three-dimensional incompressible flows in cylindrical coordinates, *J. Comput. Phys.* **123**, 402 (1996).
  - [51] F. Toschi and E. Bodenschatz, Lagrangian properties of particles in turbulence, *Annu. Rev. Fluid Mech.* **41**, 375 (2009).
  - [52] K.M.J. Alards, H. Rajaei, L. Del Castello, R.P.J. Kunnen, F. Toschi, and H.J.H. Clercx, Geometry of tracer trajectories in rotating turbulent flows, *Phys. Rev. Fluids* **2**, 044601 (2017).
  - [53] Q. Zhou, C. Sun, and K.-Q. Xia, Experimental investigation of homogeneity, isotropy, and circulation of the velocity field in buoyancy-driven turbulence, *J. Fluid Mech.* **598**, 361 (2008).
  - [54] O. Shishkina, S. Horn, S. Wagner, Falkner–Skan boundary layer approximation in Rayleigh–Bénard convection, *J. Fluid Mech.* **730**, 442 (2013).
  - [55] S. Sterl, H.-M. Li, and J.-Q. Zhong, Dynamical and statistical phenomena of circulation and heat transfer in periodically forced rotating turbulent Rayleigh–Bénard convection, *Phys. Rev. Fluids* **1**, 084401 (2016).
  - [56] H. Schlichting and K. Gersten, *Boundary-layer theory* (Springer-Verlag Berlin, Heidelberg, 2000).
  - [57] P.K. Kundu and I.M. Cohen, *Fluid Mechanics* (Academic Press, London, 2002).